ELSEVIER

Journal of Crystal Growth 210 (2000) 296–302

JOURNAL OF CRYSTAL GROWTH

www.elsevier.nl/locate/jcrysgro

Near-field photocurrent spectroscopy of laser diode devices

J.W. Tomm[a,*], T. Günther[a], Ch. Lienau[a], A. Gerhardt[b], J. Donecker[b]

[a]*Max-Born-Institut für Nichtlineare Optik und Kurzzeitspektroskopie, Max-Born-Str. 2A, D-12489 Berlin, Germany*
[b]*Institut für Kristallzüchtung, D-12489 Berlin, Germany*

Abstract

Near-field optical beam-induced current (NOBIC) experiments performed on commercial laser diode devices are presented. NOBIC and 'macroscopic' photocurrent data are compared and new results on *edge-emitting* laser devices with different waveguide architectures are analyzed. We discuss the image formation in these experiments, in particular the role of waveguiding and saturation processes. Both the ground and first excited mode of the waveguide structure are spatially resolved. The first NOBIC images of *top-emitting* vertical cavity lasers excited through the top Bragg-mirror are reported.

PACS: 42.55.P; 07.79.F; 73.50.P

1. Introduction

Photoelectric spectroscopy is a standard characterization technique for analyzing optoelectronic devices. Among others the laser (optical) beam-induced current (LBIC or OBIC, respectively) technique belongs to the toolbox of device designers and manufacturers, cf. e.g. Refs. [1,2]. Replacing the focused light of the laser beam, that is used as the LBIC excitation source, by the emission from a fiber tip of a near-field scanning optical microscope (NSOM), one achieves an excitation light spot with sub-wavelength dimension. Thus this novel technique — called 'near-field optical beam induced current (NOBIC)' — is in fact an extension of LBIC/OBIC beyond the diffraction limit.

NOBIC is a measurement that uses the '*emission mode*' of the NSOM. The investigated sample itself serves as photoelectric detector. Thus, in a first approximation, a NOBIC image mirrors the spatial distribution of the photoelectric sensitivity of a given sample such as a laser diode. For a more quantitative image analysis, processes such as minority carrier transport and wave guiding within the device have to be considered. First reports on the application of this new technique to the monitoring of threading dislocations on relaxed Ge_xSi_{1-x} films and to InGaAsP laser diode characterization have been given in 1994 by Hsu et al. and Buratto et al., respectively [3,4].

Herzog et al. reported on the application of NSOM-based experiments to *edge-emitting* laser diode characterization [5–7]. NOBIC was used for obtaining information on compositional and electronic structure of their edge emitting laser diode

* Corresponding author. Tel.: + 49-30-63921453; fax: + 49-30-63921459.

E-mail address: tomm@mbi-berlin.de (J.W. Tomm)

0022-0248/00/$ - see front matter
PII: S0022-0248(99)00700-9

structures [6,7]. Kolb et al. used NOBIC data for methodical considerations and fiber tip characterization purposes [8]. Lu et al. [9] reported on a study of visible quantum-well (QW) edge-emitting lasers using NOBIC. Our group recently introduced NOBIC as a novel method for monitoring aging processes in edge-emitting laser diodes [10–13].

NOBIC work at *vertical cavity surface emitting lasers* (VCSEL) has been reported by DeAro et al. [14]. In order to get direct access to the active region the authors investigated cleaved devices exciting at the cleaved cross sections. NSOM-based experiments of the VCSEL aperture, i.e. with observing through the upper Bragg-mirror, have been reported so far only in emission mode, i.e. for mode and polarization analysis of VCSEL devices [15,16].

In our previous work [10–13] we described and implemented NOBIC as a tool for analyzing commercial edge emitting lasers. We directed special attention to image formation processes in lasers with different waveguide architectures (such as graded and homogeneous) and coated front facets. Waveguide properties have been discussed and the ground mode of the waveguide was imaged. So far no direct experimental access to higher modes of the laser waveguide was obtained. In this paper, such data are presented for the first time. Furthermore, we address the role of saturation processes for NOBIC image formation. NOBIC and 'macroscopic' photo-current (PC) data are compared and new results obtained with *edge-emitting* laser devices with different waveguide architectures are presented. Finally, we discuss first NOBIC results obtained from *top-emitting* VCSEL devices by exciting them through the thick ($\approx 3\,\mu m$) top Bragg-mirror.

2. Experimental procedure

The NSOM used for our experiments is based on a commercial Topometrix Aurora system. The fiber probes used were obtained by etching and subsequent Al-deposition. Typical aperture diameters range between 100 and 200 nm. More details are given in Refs. [10–13]. The 'macroscopic' PC spectra are recorded either with an FT-IR-spectrometer [17] or a conventional grating monochromator [18]. In all these measurements the excitation light spot was about $\varnothing = 100\,\mu m$, i.e. the whole epitaxial layer sequence is uniformly illuminated.

The three investigated *edge-emitting structures* are laser diodes designed for the 808 and 850 nm emission range. The epitaxial layer sequences of the (In)AlGaAs/GaAlAs/GaAs structures are similar and meet the standard for step index (SIN) high-power devices, cf. e.g. Ref. [18]. The common features of all of them are the (In)GaAlAs QW active regions and about 1.5–1.7 μm wide $Al_{0.6}Ga_{0.4}As$-cladding layers on both sides of the waveguide. We compare structures with (i) a waveguide thickness of 1000 nm and a pair of off-centered QWs (Fig. 1), (ii) a thickness of 1000 nm and centered QWs (Fig. 3) and (iii) a thickness of 420 nm (QW centered, Fig. 2). All samples are anti-reflection coated with an about 120 nm thick Al_2O_3-layer.

The ion-implanted VCSEL structures follow the well-known design for *top-emitting devices*. The layer structure starts from the 7 nm thick GaAs QWs, bounded by 5 nm $Al_{0.25}Ga_{0.75}As$ barrier layers, with $Al_{0.6}Ga_{0.4}As$ cladding layers. The highly n- and p-doped Bragg-mirrors are outside of these and consist of 24 pairs with a thickness of 130 nm, in total 3.1 μm, plus another 0.1 μm of spacer layer above the active region. The diameter of the aperture is 20 μm.

3. Results

Fig. 1a shows NOBIC scans along a line perpendicular to the active layer of the SIN structure with a waveguide thickness of 1 μm and a pair of 120 nm off-centered QWs. A schematic diagram of the built-in potential is added. The sample is excited through the 120 nm thick Al_2O_3 coating layer. The parameter in these scans is the excitation wavelength, that is varied in a small range around the emission wavelength (about 808 nm). All scans show a narrow PC peak centered inside the waveguide. The spatial halfwidth of this peak increases by more than a factor of 2 as the excitation is tuned from 820 to 800 nm. Fig. 1b shows the

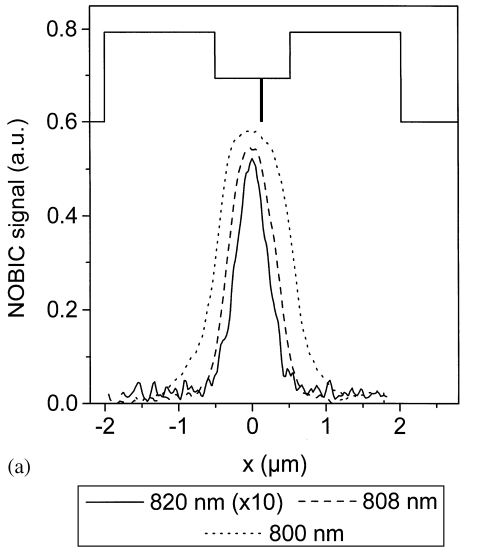

(a)

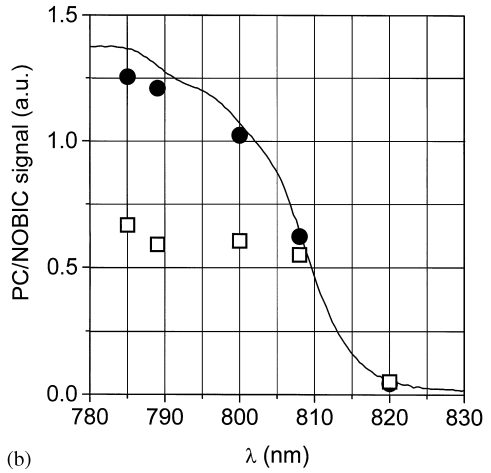

(b)

Fig. 1. NOBIC line scans obtained with different excitation wavelengths. The band diagram of the 808 nm emitting asymmetric structure is given by the full line (top). (b) 'Macroscopic' PC spectrum (full line), spatially integrated NOBIC signals (full circles) and NOBIC signal magnitude at the peak (open squares) for the same device.

spatial integral of these NOBIC scans versus wavelength (full circles) as well as the signal magnitude at the peak (open squares). The full line is the 'macroscopic' PC spectrum obtained from the same device obtained with a spatial resolution of 100 μm. We stress the close agreement between the 'macroscopic' PC spectrum and the integrated NOBIC scans.

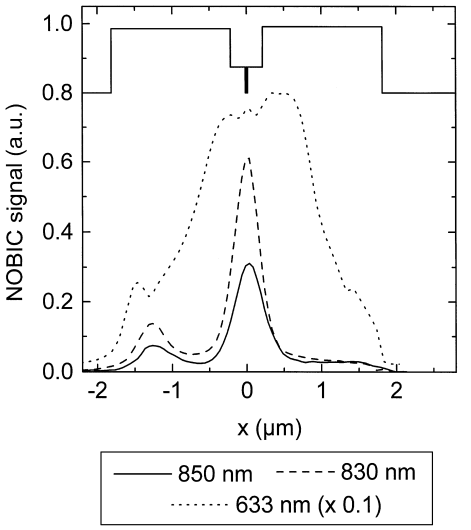

Fig. 2. NOBIC line scans obtained with different excitation wavelengths. The band diagram of the 850 nm emitting structure is given by the full line.

Fig. 2 gives NOBIC scans from a 850 nm SIN structure with a thinner 420 nm waveguide. For excitation around the QW band gap we observe again the pronounced narrow maximum at the waveguide center. In addition, in this diode, a second off-center peak is found that is spatially shifted by about 1.5 μm. For excitation high above the band gap (633 nm) we observe a strong NOBIC signal for tip positions within the wide band gap $Al_{0.6}Ga_{0.4}As$-cladding layers ($E_g \approx 2.2$ eV) that are actually transparent for the 633 nm radiation, in agreement with earlier findings [11].

Fig. 3 shows NOBIC scan data obtained from a third coated SIN laser structure with a 1 μm waveguide. The architecture of the diode is nominally identical to that of the device shown in Fig. 1 apart from the QW being centered in the waveguide. Despite this close architectural similarity the NOBIC scans are fundamentally different. In addition to the narrow central NOBIC peak we find two more peaks for excitation inside the waveguide that are spatially separated by 550–600 nm. The relative intensity of these side peaks with respect to that of the central one increases as the excitation is tuned from 820 to 780 nm.

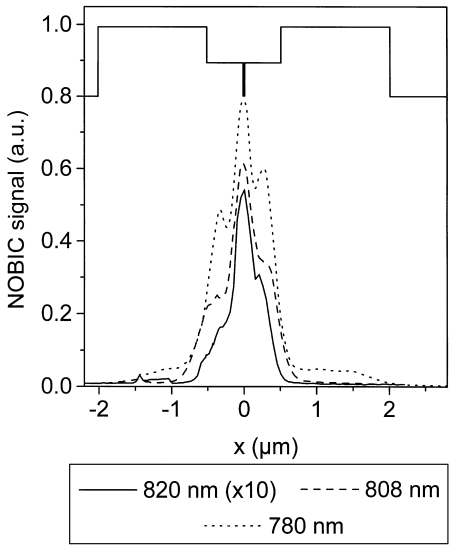

Fig. 3. NOBIC line scans obtained with different excitation wavelengths. The band diagram of the 808 nm emitting symmetric structure is given by the full line (top).

Fig. 4a shows a 'macroscopic' PC spectrum from a VCSEL measured with a spectrometer providing an light beam with an *f*-number of 10. The insert gives the detailed shape of the cavity resonance (full line) and compares it to a PC spectrum recorded with an excitation beam focused with an *f*-number of 2. Fig. 4b shows a NOBIC-map measured from the same device for 820 nm excitation near the physical edge of the $\varnothing = 20\,\mu m$ aperture of the device, whereas the shear force topography is given in Fig. 4c.

4. Discussion

The NOBIC scans on all three edge-emitting laser structures show directly that — for excitation energies around the laser photon energy — the predominant contribution to the photocurrent signal is generated with the near-field probe being positioned on top of the laser waveguide, where coupling into the waveguide is most efficient. The strong wavelength dependence of the spatially integrated NOBIC signal intensity (Fig. 1b) between 780 and 820 nm indicates that the main contribution to the photocurrent comes from carriers that are generated by interband absorption inside the QW. Different contributions to this signal have to be considered [13], among them propagating waves that are confined inside the laser waveguide by total internal reflection and unguided waves that are propagating through the laser device but are not confined to the waveguide structure. Due to the finite thickness of the 120 nm antireflection coating the contribution of purely evanescent waves is of minor importance in our experiments, as was discussed in detail in Ref. [13]. Propagating guided waves can only be excited for tip positions inside the waveguide structure and this contribution is thus spatially localized to the waveguide region. These waves penetrate deep into the waveguide structure and will be efficiently absorbed by the quantum well. In contrast, the signal from unguided propagating waves should show a weaker dependence on the position of the excitation spot. Thus the strong decrease of the NOBIC signal for tip positions outside the waveguide region indicates that — for excitation energies around the QW band gap — the contribution from unguided waves is only of minor importance. This changes as the excitation photon energy is increased beyond the QW band gap. With increasing QW absorption coefficient the relative contribution from unguided waves increases (Fig. 3, 780 nm) and gives rise to the spatially broad contribution to the NOBIC signal in Fig. 2 for excitation at 633 nm, when — additionally to the QW — the whole waveguide is excited.

The good agreement between spatially integrated near-field and macroscopic PC spectra in Fig. 2 shows that the near-field scans allow one to interpret the *microscopic origin* of far-field PC spectra. Two major contributions are revealed: (i) propagating light that is injected to the laser waveguide produces the main PC contribution at excitation energies around the QW band gap, while (ii) unconfined propagating light gives the dominant PC contribution at excitation of several hundred meV above the QW band gap.

While this general interpretation is found to hold for all investigated edge-emitting laser structures, considerable differences are found in the spatial structure of the NOBIC scans for the different

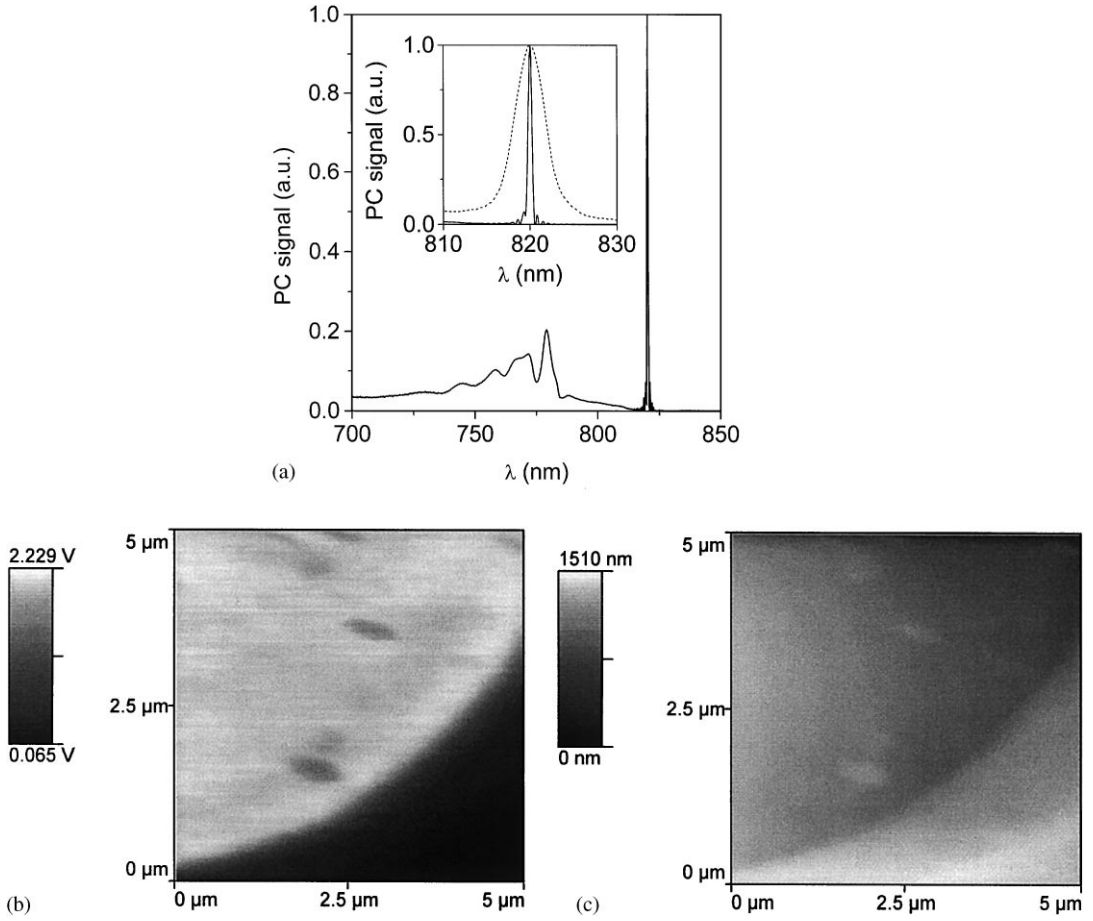

Fig. 4. (a) 'Macroscopic' PC spectrum from a 820 nm emitting VCSEL device. The inset shows the normalized main resonance measured with excitation light having different beam divergence's. (b) NOBIC map from the same 820 nm emitting VCSEL device. (c) Topographic shear force image from the 820 nm emitting VCSEL device obtained simultaneously with the NOBIC map.

devices. In the SIN structure with the off-centered QW (Fig. 1) we find that the width of the narrow PC peak increases by more than a factor of two for excitation between 820 and 800 nm. In this energy range, the QW absorption coefficient increases by more than two orders of magnitude and thus the penetration depth of the injected light in the waveguide varies strongly. This makes it likely that the observed change in spatial shape is due to a saturation of the guided wave contribution at least in center of the waveguide since these waves are completely absorbed in the laser diode for QW absorption. The same saturation effect is also seen in Fig. 3 where the intensity ratio between central peak and side wings gets smaller for decreasing wavelength.

A completely different spatial NOBIC shape is found for the SIN structure with the symmetrically centered QW (Fig. 3) where three separate peaks are spatially resolved. To a first approximation, in the absence of saturation processes, the spatial structure of the NOBIC scan reflects the intensity profile of the waveguide mode structure. The observation of three peaks indicates that, in this structure, we are not only resolving the $m = 0$ ground mode (central peak), but also the mode profile of the excited mode ($m = 1$) that gives rise to the two additional outer satellite peaks, separated by

550–650 nm. We point out that the only structural difference between the devices in Figs. 1 and 3 is the shift in the center position of the QW — otherwise the waveguide is not intentionally modified. This indicates the pronounced effect of QW position on the modal waveguide structure and highlights the sensitivity of the NOBIC scans to details of the laser waveguide architecture on a subwavelength scale.

The data in Fig. 2 for the laser with a 420 nm waveguide give a clear indication of the imperfect design of this device. In particular, the observation of pronounced QW-photosensitivity far away from the physical QW position suggests that during laser operation there are substantial losses due to a leakage of the waveguide. The asymmetric shape to the NOBIC scans at 633 nm is likely due to the different Al-mole fractions in the upper and lower claddings in this device.

The VCSEL device basically acts as a resonant cavity detector with the main PC feature spectrally situated at the cavity resonance that corresponds to the emission wavelength of the device. The interpretation of the PC spectra from VCSELs (cf. Fig. 4a) may be done in a way that is very similar to that given for edge emitters, cf. Refs. [10–13]. However, for the top emitting device the influence of the cavity formed by both Bragg-mirrors must additionally be taken into account. The mirror pattern affects the entire PC spectrum including the QW-region as well as the below-band-gap spectral region (Fig. 4a). For edge emitters, the latter one has been shown to be a sensitive indicator for monitoring defect accumulation during device operation. We find that the same holds for VCSEL devices. This will be demonstrated in Ref. [19]. In the NOBIC images we find a high uniformity of the VCSEL photosensitivity. Topographic surface features (cf. Fig. 4c) are highly spatially resolved in these images, whereas the spatial resolution of features from the active layer of the device (at a depth 3.1 μm), such as the circular structure, that is indicative for device aging [19], are less resolved as is expected from the substantial spreading of the excitation spot.

We now address the PC feature that is related to the cavity resonance. The inset in Fig. 4a shows the far-field PC spectrum around the cavity resonance for two different f-numbers of the excitation light beam. The spectral broadening is clearly caused by the fact, that the Bragg-mirror maintains its extremely high selectivity only for parallel light (f-number $= \infty$, perpendicular incidence) whereas for a strongly focused light spot with a small f-number a variety of wavelengths is transmitted. Half-width and 'contrast ratio' data are collected in Table 1. The 'contrast ratio' is defined as the PC signal ratio at the resonance and the minimum at shorter wavelengths close to the resonance. Such a contrast ratio is also determined from NOBIC images (obtained in the same way as the data given in Fig. 4b) measured for different excitation wavelengths from the same VCSEL as the shown in Fig. 4a and was found to be 3.5. Now both FWHM of the VCSEL resonance as well as 'f-number of the fiber tip' can be extrapolated and are found to be 9 meV and 0.7, respectively. Details of the analysis will be given in Ref. [19]. Thus, we demonstrate that the use of a resonant cavity detector such as a VCSEL device offers a way for characterizing the depth-dependent spatial resolution of a near-field fiber probe.

Table 1
Dependence of the VCSEL photocurrent spectrum in the spectral range of the cavity mode on the experimental conditions

f-number	FWHM (meV)	'Contrast ratio' at the cavity mode	Remark about how measured
10	0.82	250	Spectrometer
4	4.8	53	Spectrometer
2	6.9	16	Spectrometer
0.7[a]	9[a]	3.5	NSOM

[a]Extrapolated from experiments with conventional spectrometer.

5. Summary

We demonstrate the potential of near-field photocurrent spectroscopy for the analysis of commercial edge-emitting front-facet coated laser diode devices of different waveguide architecture. By comparing spatially resolved near-field and macroscopic photocurrent spectra, we identify the microscopic origin of the far-field spectra. Namely, two contributions are revealed: (i) light that is injected

into the laser waveguide is absorbed in the active QW layer and gives the major PC contribution for excitation energies around the QW band gap, (ii) unconfined propagating light gives the dominant PC contribution at excitation of several hundred meV above the QW band gap.

A comparison of near-field data for different diodes reveals the sensitivity of the technique to details of the laser waveguide architecture on a sub-wavelength scale and thus makes it a helpful tool for device manufacturers. Specifically, the spatial profile of the ground and first excited mode of a 1 μm wide step-index waveguide structure are independently resolved. With different excitation wavelengths, near-field photocurrent spectroscopy permits the *selective* testing of different building blocks of a laser device such as the quantum well and waveguide region (for excitation around the QW band gap), the cladding layers (above band-gap excitation) and defect areas for below band-gap excitation.

Acknowledgements

Financial support by the BMBF under contract 13N7384 is gratefully acknowledged.

References

[1] C.J.R. Sheppard, Scanning Miroscopy 3 (1989) 15.
[2] J. Jimenez, M.A. Gonzalez, L.F. Sanz, L.R. de Angelo, J. Bonnafe, Semicond. Sci. Technol. 7 (1992) A202.
[3] J.W.P. Hsu, E.A. Fitzgerald, Y.H. Xie, P.J. Silverman, Appl. Phys. Lett. 65 (1994) 344.
[4] S.K. Buratto, J.W.P. Hsu, E. Betzig, J.K. Trautman, R.B. Bylsma, C.C. Bahr, M.J. Cardillo, Appl. Phys. Lett. 65 (1994) 2654.
[5] W.D. Herzog, M.S. Ünlü, B.B. Goldberg, G.H. Rhodes, C. Harder, Appl. Phys. Lett. 70 (1997) 688.
[6] M.S. Ünlü, B.B. Goldberg, W.D. Herzog, D. Sun, E. Towe, Appl. Phys. Lett. 67 (1995) 1862.
[7] B.B. Goldberg, M.S. Ünlü, W.D. Herzog, H.F. Ghaemi, E. Towe, IEEE J. Selected Topics Quant. Electron. 1 (1995) 1073.
[8] G. Kolb, K. Karrai, G. Abstreiter, Appl. Phys. Lett. 65 (1994) 3090.
[9] N.H. Lu, D.P. Tsai, F.C. Yeh, C.S. Chang, T.T. Tsong, M.F. Huang, C.J. Liu, SPIE Proc. 3285 (1998) 59.
[10] A. Richter, J.W. Tomm, C. Lienau, J. Luft, Appl. Phys. Lett. 69 (1996) 3981.
[11] A. Richter, Ch. Lienau, J.W. Tomm, Surface Interface Anal. 25 (1997) 573.
[12] J.W. Tomm, A. Richter, Ch. Lienau, T. Elsaesser, J. Luft, SPIE Proc. 3001 (1997) 29.
[13] Ch. Lienau, A. Richter, J.W. Tomm, Appl. Phys. A 64 (1997) 341.
[14] J.A. DeAro, K.D. Weston, R.W. Herrick, P.M. Petroff, S.K. Buratto, Semicond. Sci. Technol. 13 (1998) 1364.
[15] I. Hörsch, R. Kusche, O. Marti, B. Weigl, K.J. Ebeling, J. Appl. Phys. 79 (1996) 3831.
[16] G.H. Van der Rohdes, J.M. Pomeroy, M.S. Ünlü, B.B. Goldberg, K.J. Knopp, D.H. Christensen, Appl. Phys. Lett. 72 (1998) 1811.
[17] J.W. Tomm, A. Jaeger, A. Bärwolff, T. Elsaesser, A. Gerhardt, J. Donecker, Appl. Phys. Lett. 71 (1997) 2233.
[18] J.W. Tomm, A. Bärwolff, U. Menzel, M. Voß, R. Puchert, T. Elsaesser, F.X. Daiminger, S. Heinemann, J. Luft, J. Appl. Phys. 81 (1997) 2059.
[19] J.W. Tomm, A. Bärwolff, T. Elsaesser, Photonics West 2000 Conference, San Jose, CA, January 23–28, 2000, SPIE Proc. 3946 (2000), in press.